CHEMICAL INTERACTIONS AND REACTION KINETICS OF THE $Ba_2YCu_3O_{6+x}$ /CeO_2 SYSTEM

W. Wong-Ng, L.P. Cook, P. Schenck, I. Levin, Z. Yang, Q. Huang, and J. Frank
Materials Science and Engineering Laboratory
National Institute of Standards and Technology
Gaithersburg, MD 20899

ABSTRACT

Chemical interactions between the $Ba_2YCu_3O_{6+x}$ superconductor and the CeO_2 buffer layers employed in coated conductors have been modeled experimentally by investigating phase equilibria in the $Ba_2YCu_3O_{6+x}$ - CeO_2 system, and also by studying the kinetics of the reaction between $Ba_2YCu_3O_{6+x}$ and CeO_2. The $Ba_2YCu_3O_{6+x}$ - CeO_2 join within the BaO-Y_2O_3-CeO_2-CuO_x quaternary system is non-binary. At 810 °C and p_{O2} = 100 Pa, at a mole ratio of $Ba_2YCu_3O_{6+x}$: CeO_2 = 40 : 60, a phase boundary was found to separate two four-phase regions. On the $Ba_2YCu_3O_{6+x}$-rich side of the join, the four-phase region consists of $Ba_2YCu_3O_{6+x}$, $Ba(Ce_{1-z}Y_z)O_{3-x}$, BaY_2CuO_5, and Cu_2O; on the CeO_2 rich side, the four phases were determined to be $Ba(Ce_{1-z}Y_z)O_{3-x}$, BaY_2CuO_5, Cu_2O and CeO_2. There appears to be negligible solid solution formation of the types $Y_{1-z}Ce_zO_{3-x}$ and $Ce_{1-z}Y_zO_{2-x}$. The minimum melt temperature along the $Ba_2YCu_3O_{6+x}$ - CeO_2 join was determined to be ≈ 860 ºC. The $Ba_2YCu_3O_{6+x}$ /CeO_2 reaction is limited by solid-state diffusion, and the reaction kinetics obeys the parabolic rule, $x = Kt^{1/2}$ (where x is thickness of the reaction layer, t is time, and K is a constant related to the reaction rate); K was determined to be 3.6 x 10^{-2} μm/$min^{1/2}$ at 830 ºC.

INTRODUCTION

With increased demand for electrical power, energy shortages and electricity outages have become common global problems. There are clear needs for improvement in electrical distribution grids and for more efficient utilization of energy resources. High-temperature superconductors have demonstrated potential for meeting these needs [1]. Consequently, there is an accelerated effort within the high T_c community on research and development of coated conductors for wire/tape applications [2-8]. These conductors are based on $Ba_2YCu_3O_x$ (Y-213) and $Ba_2RCu_3O_x$ (R=lanthanides) as the principal superconducting materials. They can be deposited on flexible metallic tapes, and the resulting materials show excellent current-carrying capability.

Specially prepared substrates form the basis for coated conductor fabrication. The two state-of-the-art technologies for producing biaxially-textured substrates are commonly known as ion beam assisted deposition (IBAD) [2-3], developed at Los Alamos National Laboratory, and rolling assisted bi-axially textured substrate (RABiTS) [4-8], developed at Oak Ridge National Laboratory. Typically, the architecture of a RABiTS film includes a number of layers of different materials deposited on the biaxially textured metallic substrate. These layers are the seed layer, barrier layer, lower cap layer, superconductor layer, and another cap layer on the superconductor [9]. The seed layer provides a thin epitaxial layer for protecting the substrate from oxidation during deposition of barrier layer. The barrier layer is a thick epitaxial layer for providing a physical/chemical barrier to substrate oxidation and substrate reaction with the superconductor layer. The lower cap layer provides additional protection for the superconductor film from

chemical reaction, and also provides texture for crystallographic alignment. Examples of lower cap layer include CeO_2, $LaMnO_3$, $SrTiO_3$, Gd_3NbO_7, and $SrRuO_3$. The two most extensively used materials have been CeO_2 and $SrTiO_3$.

For a given combination of buffer layers that has been found to promote epitaxial growth of $Ba_2YCu_3O_{6+x}$, there may be unavoidable reactions at the interface between layers. Understanding of interfacial reactions of Y-213 phase with the buffer layers will provide information about how to avoid and/or control the formation of second phases. Phase equilibrium data will allow better interpretation of the results of TEM analysis of coated conductor interfaces.

This report describes the phase equilibria of the multi-component systems representing the interaction of $Ba_2YCu_3O_{6+x}$ with CeO_2 [10, 11], and also the kinetic study of phases formed at the interface. Phase equilibria and structural characterization studies were conducted by x-ray and neutron diffraction, and differential thermal analysis/thermal gravimetric analysis (DTA/TGA) [12]. Kinetic studies were conducted by depositing the Y-213 superconductor on polished CeO_2 pellets using pulsed laser deposition (PLD). X-ray diffraction and TEM were used for characterization of phase formation and to determine the thickness of the product layer.

EXPERIMENTAL[1]

Phase equilibria

(1) *Preparation of samples in the $Ba_2YCu_3O_{6+x}$-CeO_2 system*

For phase equilibra studies, a master batch of the superconductor phase $Ba_2YCu_3O_{6+x}$ was prepared by heating a mixture of BaO, Y_2O_3 and CuO under purified air (CO_2- and H_2O-scrubbed). The BaO starting material was produced from $BaCO_3$ (99.99 % purity, metals basis) by vacuum calcination in a vertical tube furnace. The following heating schedule was used: room temperature to 1300 °C in 20 h; isothermal at 1300 °C for 10 h; 1300 °C to room temperature in 20 h. To prepare $Ba_2YCu_3O_{6+x}$, stoichiometric amounts of BaO, Y_2O_3 and CuO were weighed out, well mixed and calcined in an atmospherically controlled high temperature furnace first at 850 °C, then at 930 °C repeatedly with intermediate grindings for about two weeks. Subsequently, thirteen samples with different ratios of $Ba_2YCu_3O_{6+x}$: CeO_2 were then prepared using the master $Ba_2YCu_3O_{6+x}$ batch and CeO_2 (5:95, 10:90, 20:80, 30:70, 35:65, 40:60, 45:55, 50:50, 60:40, 70:30, 80:20, 90:10, and 95:5). The processes of sample weighing, sample homogenization and pellet-pressing were performed inside a glove-box. Pelletized samples were placed inside individual MgO crucibles for annealing in a horizontal box-type controlled-atmosphere furnace. Transfer from the glove-box to the box furnace and vice versa was achieved via a second transfer vessel and an interlock system attached to the furnace.

(2) *Determination of the ternary phase diagrams*

Stoichiometric amounts of BaO, CeO_2, CuO and Y_2O_3 (99.99 % purity, metals basis) were first weighed inside a dry box according to the proper mole ratio, and were then mixed and pressed into pellets, followed by annealing in a controlled-atmosphere furnace. Sample transfer was accomplished by using an air-tight vessel. During the annealings, the oxygen pressure of Ar/O_2 mixtures was controlled using a mass flow meter and monitored at both the inlet and outlet of the furnace using a zirconia oxygen sensor. Samples were studied under

[1] Certain trade names and company products are mentioned in the text or identified in illustrations in order to adequately specify the experimental procedures and equipment used. In no case does such identification imply recommendation or endorsement by the National Institute of Standards and Technology.

atmospherically-controlled conditions at 810 ºC with p_{O2} = 100 Pa (0.1 % O_2 by volume fraction) (in the absence of CO_2). Intermediate grindings and pelletizings took place until no further changes were detected in the powder x-ray diffraction patterns. Samples were processed for about 3 weeks each.

(3) *X-ray and neutron diffraction*

X-ray powder diffraction was used to identify the phases synthesized, to confirm phase purity, and to determine phase relationships. All x-ray patterns were measured using a hermetic cell designed for air-sensitive materials [13]. A computer-controlled automated diffractometer equipped with a θ-compensation slit and CuK_α radiation was operated at 45 kV and 40 mA. The radiation was detected by a scintillation counter and a solid-state amplifier. The Siemens software package and the reference x-ray diffraction patterns of the Powder Diffraction File (PDF) [14] were used for performing phase identification.

One selected sample within the $Ba(Ce_{1-z}Y_z)O_{3-x}$ solid solution (discussed later) was studied using neutron diffraction. Neutron diffraction data were collected with the 32 detector BT-1 diffractometer at the National Institute of Standards and Technology (NIST) Center for Neutron Research using a Cu(311) monochromator (λ=1.5396(1) Å). A 6 g sample was sealed into a 6 mm diameter vanadium container. Measurements were made at room temperature. The structural refinement was performed by using the GSAS software suite [15]. The structure of $BaCeO_3$ was employed as the initial model for the refinements [16].

(4) *Differential thermal analysis/Thermogravimetric Analysis (DTA/TGA)*

Simultaneous differential thermal analysis and thermogravimetric analysis (DTA/TGA) were used to study thermal events. Most experiments utilized primarily the DTA signal; the TGA signal was useful primarily in following oxygen gain/loss associated with the CuO_x component. DTA/TGA experiments were performed using an electronically upgraded Mettler TA-1 system fitted with an Anatech digital control and readout system. The DTA/TGA apparatus was calibrated against the α/β quartz transition (571 °C) and the melting point of NaCl (801 °C), and temperatures reported in this study have a standard uncertainty of ± 5 °C. Event temperatures were determined as the intersection of the baseline with the extrapolated linear portion of the rising DTA peak. Oxygen partial pressure during DTA/TGA was controlled using an analyzed Ar/O_2 mixtures. During the experiments, gas was continuously flowed through the sample region at a rate of 150 mL/min, and the oxygen pressure at the outlet of the DTA/TGA system was periodically checked with a zirconia sensor.

Kinetic studies

Kinetic studies were conducted by depositing the Y-213 superconductor on polished CeO_2 pellets (obtained from Alfa Aesar) using pulsed laser deposition (PLD).

(1) *Pulsed Laser Deposition Facility (Fig. 1)*

The laser deposition process is a high energy process with high deposition rates. Complex target compositions can be used, provided congruent vaporization occurs, with stoichiometric material transfer. The details of the experiments are as follows: excimer laser (248 nm, 100 mJ, and 10 Hz); deposition distance (3 cm); process gas (6.7 Pa oxygen); deposition rate (≈ 11.5 nm/min); and film thickness (≈ 570 nm).

(2) *Procedure*

To study the kinetics of reaction, a preliminary study to obtain the appropriate temperature range for heat treatments was first conducted. Seven films were prepared by PLD for this study, four for the preliminary studies to obtain the appropriate heat-treatment temperatures. Heat treatments were subsequently conducted in air at 790 °C, 810 °C, and 830 °C. For each sample, each subsequent cumulative heat treatment was in general doubled in time. X-ray diffraction was used to obtain intensity of selected reflections of these samples. The intensity values are assumed to be proportional to the amount of a particular phase, or the thickness of the reaction layer. Transmission electron microscopy (TEM) study was carried out to obtain microstructure, including identification of phases and thickness of reaction layer. From these observations, a kinetic model describing the progress of reaction could be determined.

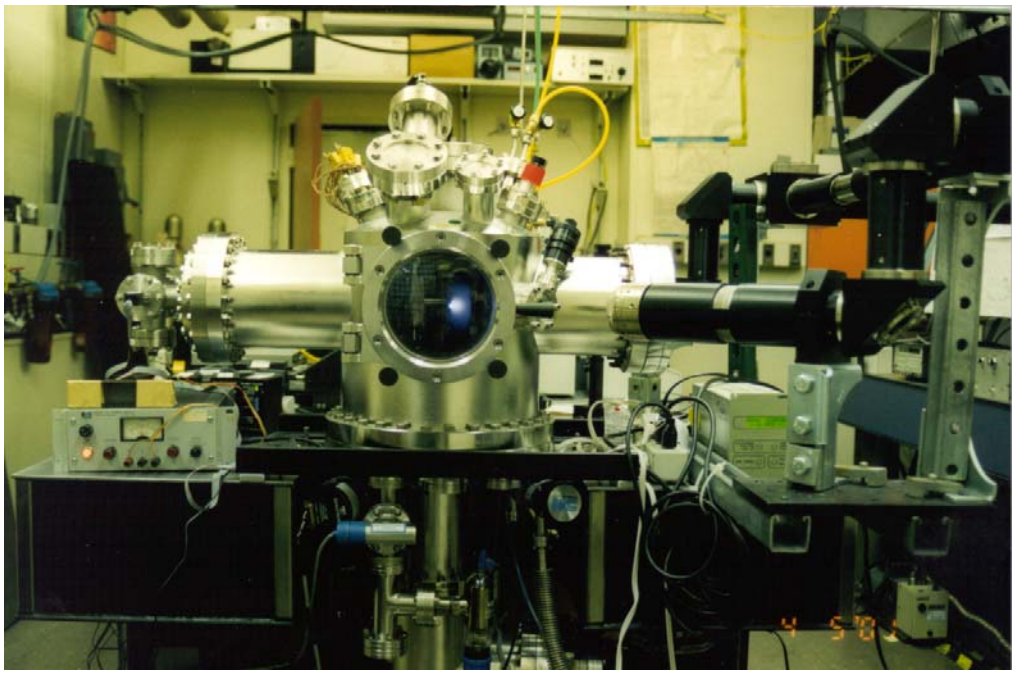

Fig. 1. NIST Pulse Laser Deposition Facility

RESULTS AND DISCUSSION

Phase equilibria between $Ba_2YCu_3O_{6+x}$ and CeO_2

Figure 2 illustrates the equilibria along the $Ba_2YCu_3O_{6+x}$-CeO_2 join in the context of the BaO-½Y_2O_3-CuO_x-CeO_2 framework. It is seen clearly that two tetrahedral volumes (4-phase regions) corresponding to $Ba_2YCu_3O_{6+x}$-$BaCeO_3$-BaY_2CuO_5-Cu_2O and $BaCeO_3$-BaY_2CuO_5-Cu_2O-CeO_2 are mutually consistent and do not overlap. BaY_2CuO_5 is commonly known as the 'green phase'. These two tetrahedra share a common plane defined by BaY_2CuO_5, Cu_2O and $BaCeO_3$. In other words, as a composition vector passes through the two tetrahedra, only three phases are observed at the boundary. This phase boundary exists at the mole ratio of $Ba_2YCu_3O_{6+x}$: CeO_2 = 40 : 60. On the $Ba_2YCu_3O_{6+x}$-rich side, the four phases possible as a result of chemical interaction were found to be $Ba_2YCu_3O_{6+x}$, $BaCeO_3$, BaY_2CuO_5, and Cu_2O; whereas at the CeO_2 rich side, the four phases are $BaCeO_3$, BaY_2CuO_5, CeO_2 and Cu_2O. Apparently Cu_2O is more stable than CuO at p_{O2} = 100 Pa, in agreement with calculated CuO/Cu_2O equilibria [17].

Cerium is known to possess various oxidation states (+2, +3 and +4), therefore CeO_{2-x} undergoes a complex oxidation/reduction chemistry under different oxygen partial pressures. Under the conditions of the present study, CeO_2 is the only stable form of cerium oxide. The $BaCeO_3$ phase is a solid solution and is more appropriately written as $Ba(Ce_{1-z}Y_z)O_{3-x}$, although it is represented as a point compound on Fig. 2 as an approximation. Figure 3 gives the subsolidus diagram of the BaO-Y_2O_3-CeO_2 system that was determined using BaO as a starting component. Along the BaO-Y_2O_3 side, only two phases were found, namely, BaY_2O_4 and $Ba_3Y_4O_9$. There is no new ternary phase in this system except for the solid solution of the Y-doped $BaCeO_3$ phase, $Ba(Ce_{1-z}Y_z)O_{3-x}$. The range of this solid solution was determined to be rather small, namely, $0 \leq z \leq 0.13$. We have studied the structure of a solid solution member using neutron diffraction, which has essentially a perovskite-related structure. Despite extensive solid solution formed at higher temperature (for example, 20.5 % mole fraction of yttria in ceria at 1500 ºC in air) [18-20], under ≈ 810 ºC and p_{O2} = 100 Pa, we found no significant solid solution of between Y_2O_3 and CeO_2.

The structure of $Ba(Ce_{1-z}Y_z)O_{3-x}$ is of the perovskite type (Fig. 4). Y was found to substitute for the Ce site with an occupancy of 0.06(2), giving rise to the unit cell content of $Ba_4(Ce_{3.76}Y_{0.24})O_{11.36}$, or the chemical formula of $Ba(Ce_{0.94}Y_{0.06})O_{2.84}$, with Z=4, (space group of *Pmcn*, a = 8.7817(4) Å, b = 6.2360(4) Å, and c = 6.2190(3) Å, V = 340.57 $Å^3$, and a density 6.236 g/cm^3). The structure consists of corner-sharing [CeO_6] octahedral rotated around the a-, b-axes (10º to 11º), and the c-axis (1.2º). Ba atoms are situated in the interstices. As the sample was prepared under 0.1 % O_2, the oxygen content was determined to be less than the value of 3.0 from neutron diffraction study. A charge balance calculation leads to the chemical formula of $Ba(Ce^{3+}_{0.26}Ce^{4+}_{0.68}Y_{0.06})O_{2.84}$.

The phase diagrams of the CeO_2-Y_2O_3-CuO_x and the BaO-CeO_2-CuO_x systems are very simple, no ternary phase or solid solution was found in these systems under 0.1% O_2 and 810 °C. The details will be published elsewhere [21].

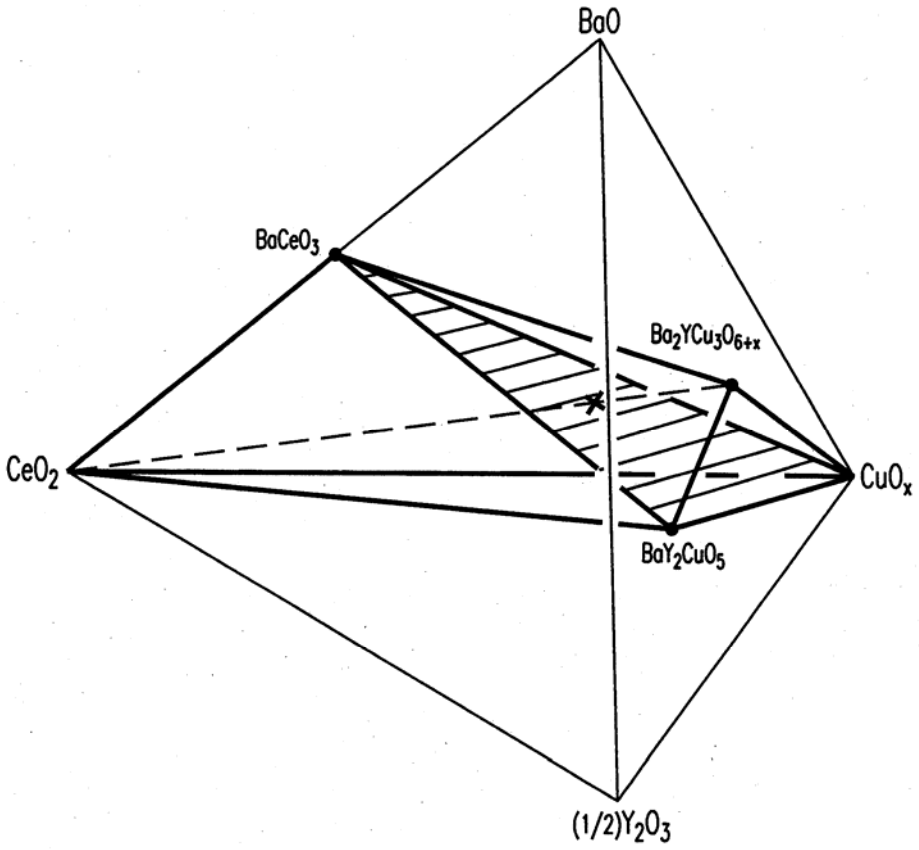

Fig. 2. The BaO-Y_2O_3-CuO_x-CeO_2 tetrahedron showing the two sub-volumes $Ba_2YCu_3O_{6+x}$-$Ba(Ce,Y)O_{3-x}$- BaY_2CuO_5- Cu_2O and $BaCeO_3$-BaY_2CuO_5- Cu_2O-CeO_2
within which the compositions of the $Ba_2YCu_3O_{6+x}$-CeO_2 join lie. "$BaCeO_3$ " is

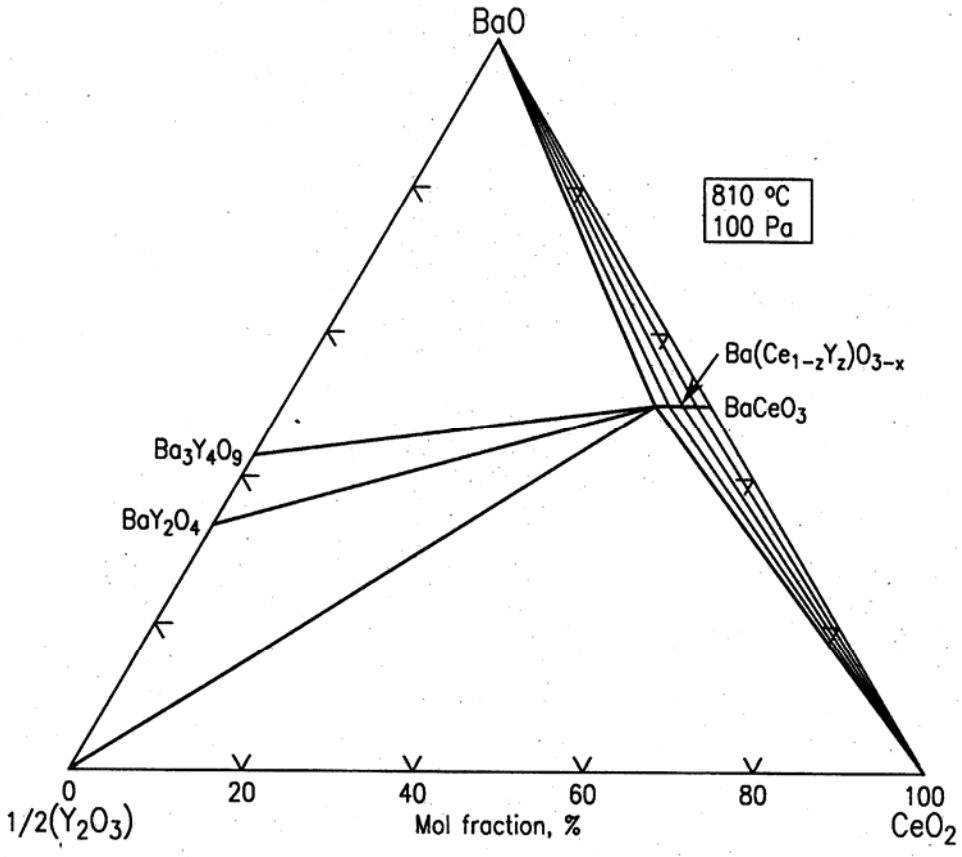

Fig. 3. Subsolidus diagram of the BaO-Y_2O_3-CeO_2 system determined at 810 °C, p_{O2}=100 Pa using BaO starting material.

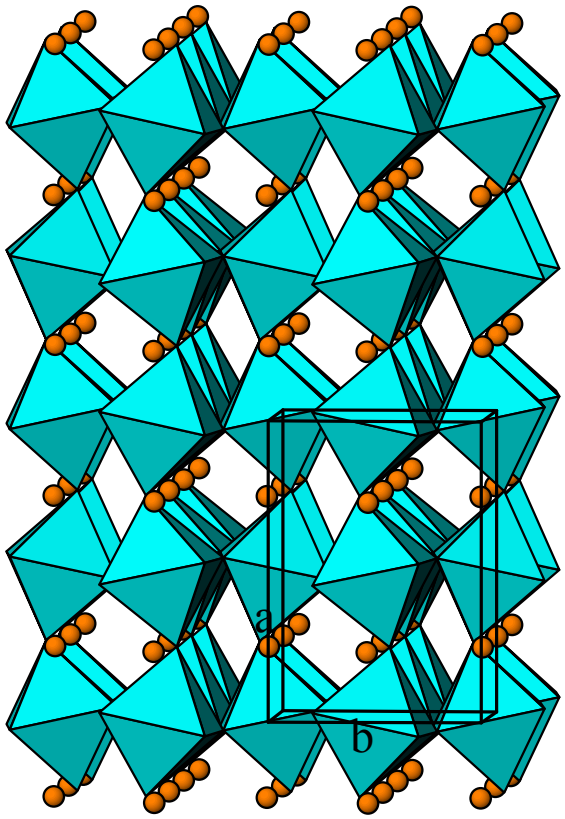

Fig. 4. Crystal structure of $Ba(Ce_{0.94}Y_{0.06})O_{2.84}$ viewed along *c*-

The initial melt temperature of the thirteen compositions can be categorized into two groups. Compositions of Y-213:CeO_2 ratio of 90:10, 80:20, 70:30, 60:40, and 45:55 gave an average melting temperature of 860 ºC. Compositions with Y-213:CeO_2 ratio of 40:60, 30:70, 20:80 and 10:90 gave an average melting temperature of 959 ºC. Therefore the minimum melting temperature of this non-binary join occurs near the $Ba_2YCu_3O_{6+x}$ side, and is estimated to take place according to the following reaction,

$$Ba_2YCu_3O_{6+x} + Cu_2O + BaY_2CuO_5 + Ba(Ce_{1-z}Y_z)O_{3-x} \rightarrow L \quad (\approx 860\ ºC).$$

The next-lowest melting temperature event occurred at ≈ 959 ºC (near the CeO_2 side). On the basis of these observations, since coated conductor processing takes place below 800 ºC, the interaction of $Ba_2YCu_3O_{6+x}$ with CeO_2 will not cause melting during processing, unless significant surface energy effects exist.

Kinetic study of $Ba_2YCu_3O_{6+x}/CeO_2$

Figure 5 shows an optical image of two pellets, CeO_2 and CeO_2 coated with PLD $Ba_2YCu_3O_{6+x}$. The latter is typical of samples used in the kinetic studies.

Figure 6 shows the x-ray patterns of a sample heat-treated at 830 °C at various lengths (expressed in minutes) of heat treatment. One can follow the intensity development of peaks related to the products of $Ba(Ce_{1-z}Y_z)O_{3-x}$, BaY_2CuO_5, and reactant phase $Ba_2YCu_3O_{6+x}$. The decrease of the peak intensity of the reactant $Ba_2YCu_3O_{6+x}$ phase (by following reflection 031), and the increase of intensity of the products $Ba(Ce_{1-z}Y_z)O_{3-x}$ (reflection 213), and BaY_2CuO_5 (reflection 131) as a function of time, is evident. We observe a linear portion of the curves followed by an almost flat section at a longer duration time. A similar intensity trend was also observed for the 810 °C experiments. The increase of intensity of the peaks as a function of time again indicates the increased formation of $Ba(Ce_{1-z}Y_z)O_{3-x}$ and the green phase due to the reaction of $Ba_2YCu_3O_{6+x}$ with CeO_2.

In most ceramic reactions there is a reaction interface between reacting phases [22]. The overall process involves (1) transport of material to the interface, (2) reaction at the interface, and (3) sometimes transport of reaction products away from the interface. The two general classes of heterogeneous reactions are those controlled by transport rate, and those controlled by phase boundary reaction rate. For a reaction in which a compound is formed as the planar reaction layer and the rate of product formation is controlled by diffusion through the product layer, then the parabolic rate law, $x = Kt^{1/2}$, is observed, where 'x' is the thickness of the reaction layer, 't' is time, and K is a constant related to reaction rate (for the rare-limiting diffusion process).

We indeed found in all three temperatures that we studied, that the parabolic rate law was obeyed. The plots of intensity vs. $(time)^{1/2}$ for the experiments at 810 °C are shown in Fig. 7. For the products $Ba(Ce_{1-z}Y_z)O_{3-x}$ and BaY_2CuO_5, the curves are rather similar. There is the straight-line portion of these curves at a relatively short reaction time period, and then the change of

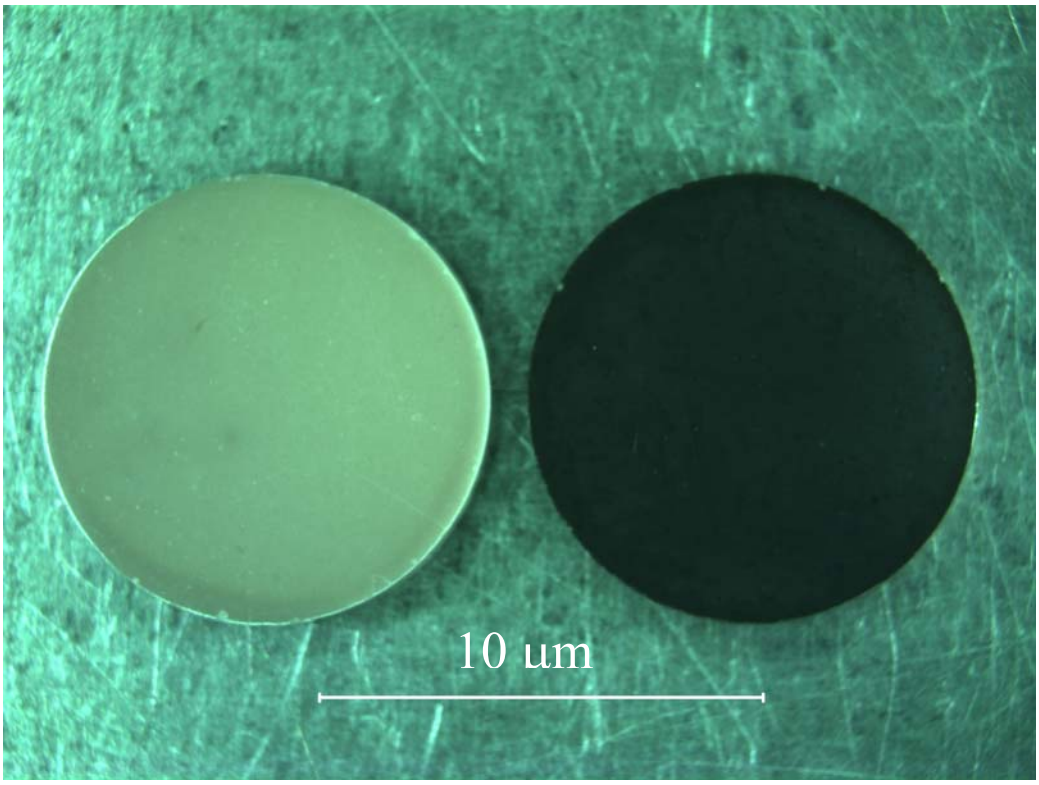

Fig. 5. Optical images of uncoated CeO_2 (left) and $Ba_2YCu_3O_{6+x}/CeO_2$ (right)

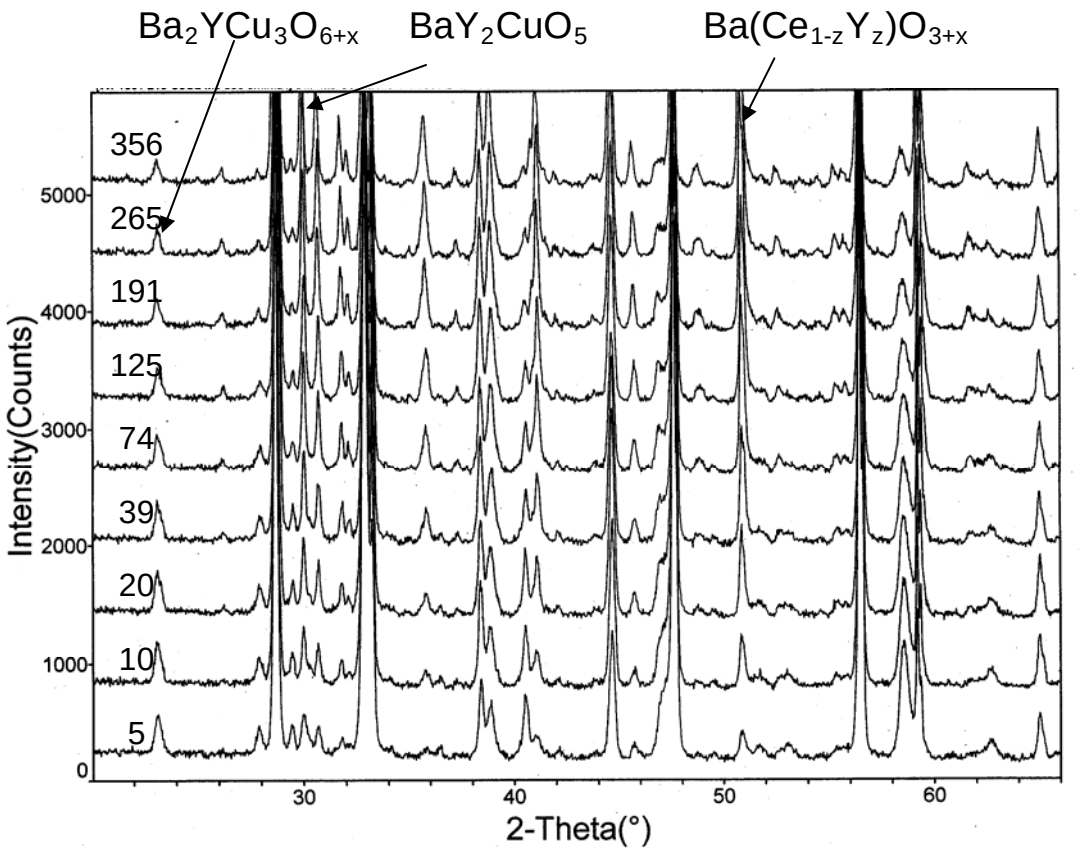

Fig. 6. Sequential x-ray diffraction patterns of $Ba_2YCu_3O_{6+x}/CeO_2$ pellet heat-treated at 830 °C for increasing cumulative time (minutes)

intensity as a function of time decreases dramatically. While the intensity of peaks corresponding to the reaction products increases, that of the reactant, namely the Y-213, decreases. The intensity vs. $t^{1/2}$ plots for the experiments at 830 °C are similar to those of 810 °C, namely, the straight-line portion of the curves for the products take place at a short range of reaction time, and then the slope becomes flat.

When one compares the phase formation features of $Ba(Ce_{1-z}Y_z)O_{3-x}$ at the three temperatures, different rates of formation are clear (Fig. 8). For example, at a higher temperature of 830 °C, the formation of $Ba(Ce_{1-z}Y_z)O_{3-x}$ was the fastest, as expected. The formation of $Ba(Ce_{1-z}Y_z)O_{3-x}$ was complete at about 180 min. At 810 °C the corresponding time was somewhat longer at 530 min. However, at 790 °C, the reaction still continues even at 3600 min. In other words, the reaction is still in the linear portion of the rate curve.

A bright-field TEM image of a cross-section of a sample heat-treated at 830 °C for 123 minutes is shown in Fig. 9. Electron energy loss spectroscopy/energy dispersive spectroscopy (EELS/EDS) measurements in TEM confirmed that the reaction layer, which is about 0.4 μm thick, consists of $Ba(Ce_{1-z}Y_z)O_{3-x}$. A mixture of Y-213, green phase, and CuO was observed in the immediate vicinity of $Ba(Ce_{1-z}Y_z)O_{3-x}$, whereas the outer part of the film consisted primarily of Y-213. Using the thickness of 0.40 μm, the parabolic equation gives a value of 3.6×10^{-2} $\mu m/min^{1/2}$ for K.

SUMMARY

We have studied the reaction of $Ba_2YCu_3O_{6+x}/CeO_2$ with respect to phase equilibria and kinetics. The reaction involves two 4-phase fields and the reaction products are $Ba(Ce_{1-z}Y_z)O_{3-x}$, BaY_2CuO_5, and CuO/Cu_2O. The minimum melting between $Ba_2YCu_3O_{6+x}$ and CeO_2 was determined to be 860 ºC. Since coated conductor processing takes place below 800 ºC, the interaction of $Ba_2YCu_3O_{6+x}$ with CeO_2 will not cause melting during processing, unless significant surface energy effects exist. We also followed the kinetics of reaction by monitoring the products $Ba(Ce_{1-z}Y_z)O_{3-x}$ and BaY_2CuO_5 as a function of time, and temperature. The reaction kinetics follows a simple parabolic rate law, characteristic of diffusion-limited processes. Further studies of interfacial reactions of $Ba_2YCu_3O_{6+x}$ with $SrTiO_3$ and with Gd_3NbO_7 are planned.

ACKNOWLEDGEMENTS

This project was partially supported by the U.S. Department of Energy. Nils Swanson of NIST is thanked for his graphical assistance. Mr. Edward Nie helped with the substrate preparation. We also acknowledge the valuable contributions from our colleagues, Drs. A. Goyal, M. Paranthaman, and R. Feenstra from Oak Ridge National laboratory, and Dr. T. Holesinger from Los Alamos National Laboratory.

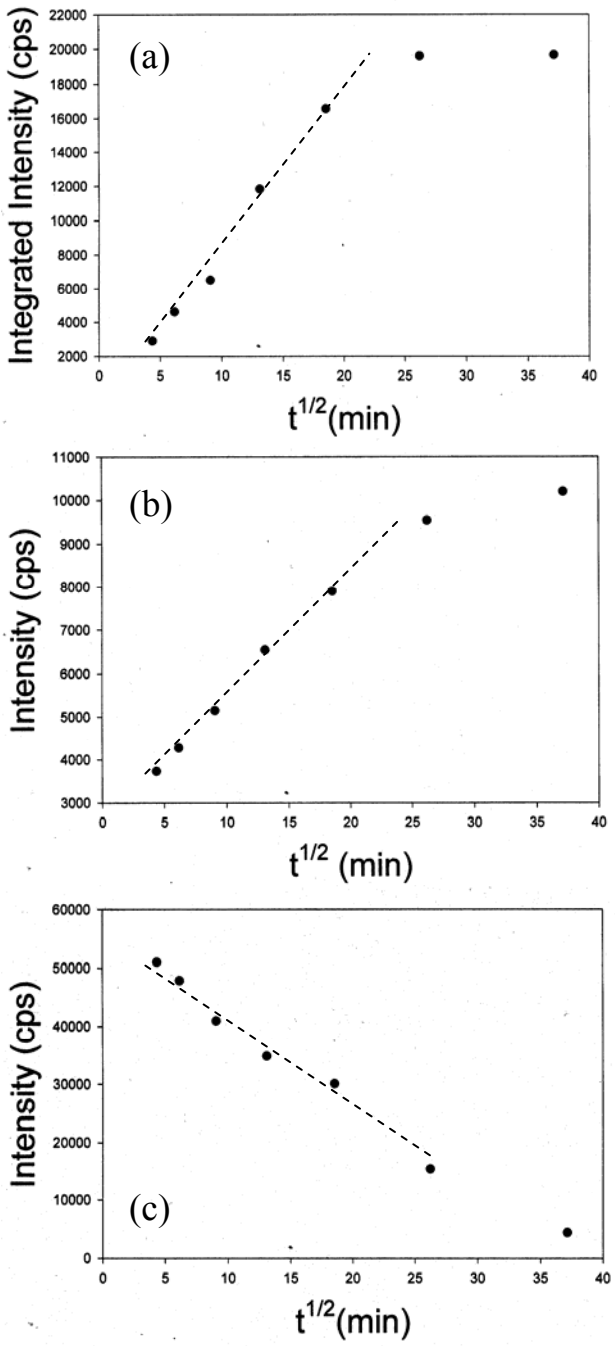

Fig. 7. Plots of intensity vs. (time, minutes)$^{1/2}$ (a) $Ba(Ce_{1-z}Y_z)O_{3-x}$, (213), (b) BaY_2CuO_5 (131), and (c) $Ba_2YCu_3O_{6+x}$ (031) for sample heat-treated at 810 °C. 'cps' stands for counts per second

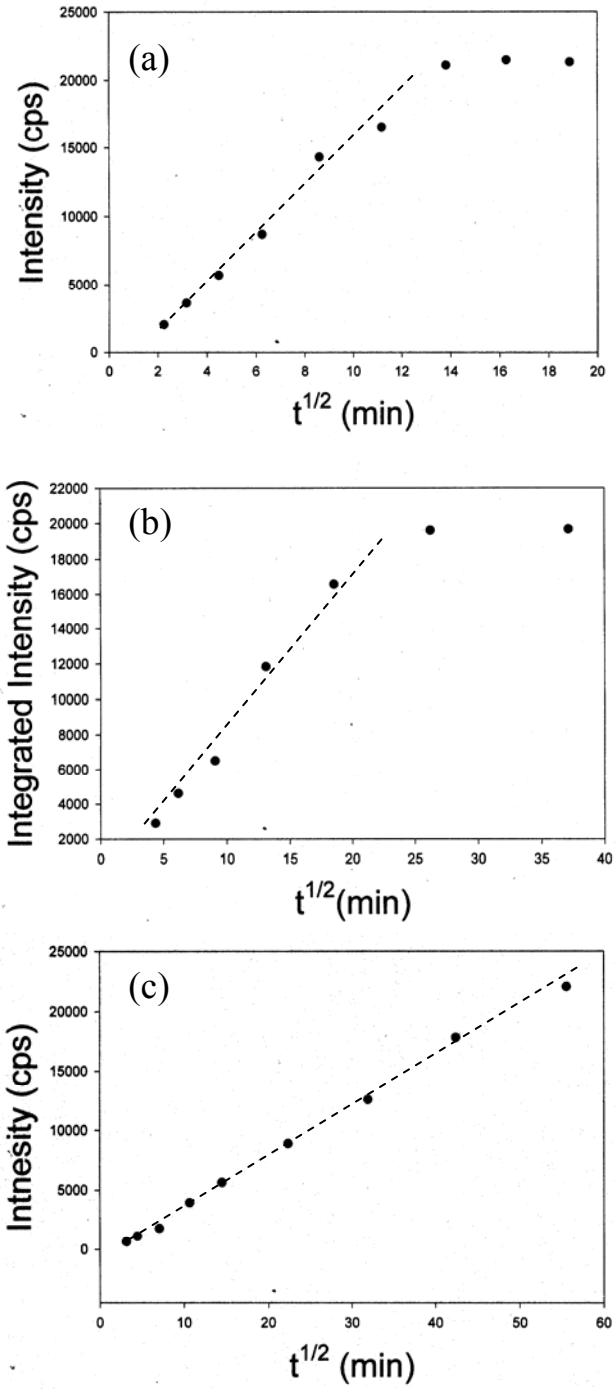

Fig. 8. Plots of intensity vs. (time, Minutes)$^{1/2}$ of $Ba(Ce_{1-z}Y_z)O_{3-x}$ (213) at three different temperatures, (a) 830 °C, (b) 810 °C, and (c) 790 °C. 'cps' stands for counts per second

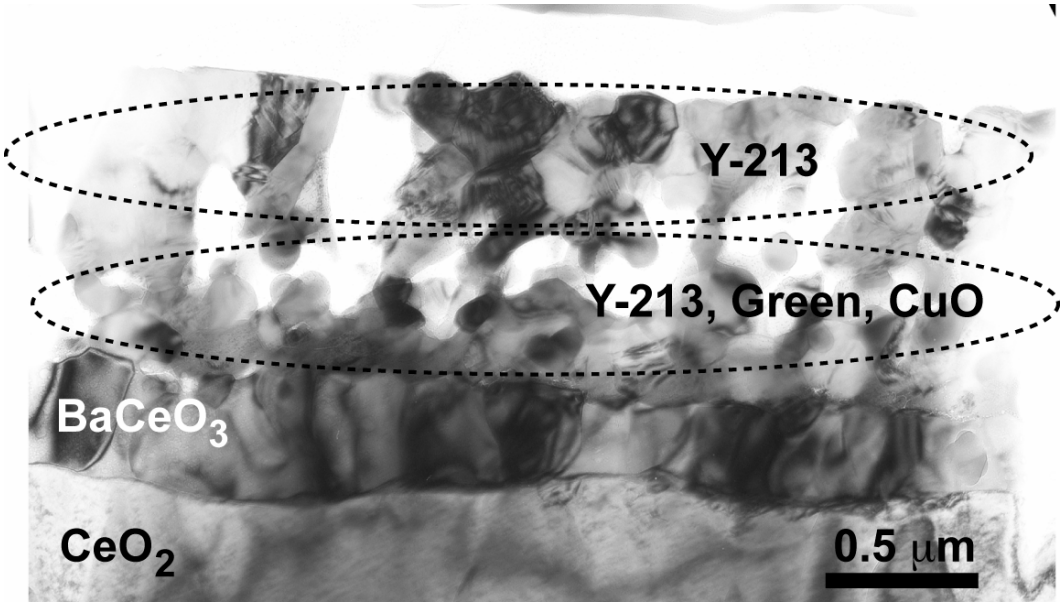

Fig. 9. Bright-field TEM image of a cross-section of a sample heat-treated at 830 °C for 123 minutes

REFERENCES

[1] US Department of Energy high temperature superconductivity program; for details, visit web site http://www.eere.energy.gov/EE/power_superconductivity.html

[2]Foltyn S.R., Peterson E.J., Coulter J.Y., Arendt P.N., Jia Q.X., Dowden P.C., Maley M.P., Wu X.D., Peterson D.E., J. Mater. Res. **12** 2941-2946 (1997).

[3] Iijima Y., Hosaka M., Tanabe N., Sadakata N., Saitoh T., Kohno O., Takeda K., J. Mater. Res. **12** 2913-2923 (1997).

[4] Malozemoff A.P., Annavaraou S., Fritzemeier L., Li Q., Prunier V., Rupich M., Thieme C., Zhang W., Goyal A., Paranthaman M., and Lee D.F., Supercond. Sci. Technol. **13** 473-476 (2002).

[5] Paranthaman M, Park C., Cui X, Goyal A., Lee D.F., Martin P.M., Chirayil T.G., Verebelyi D.T., Norton D.P., Christen D.K., and Kroeger D.M., J. Mater. Res **15** (12) 2647-2652 (2000).

[6] Goyal A., Lee D.F., List F.A., Specht E.D., Feenstra R., Paranthaman M., Cui X., Lu S.W., Martin P.M., Kroeger D.M., Christen D.K., Kang B.W., Norton D.P., Park C., Verebelyi D.T., Thompso J.R., Williams R.K., Aytug T., and Cantoni C., Physica C **357** 903-913 (2001).

[7] Aytug T., Goyal A., Rutter N., Paranthaman M., Thompson J.R., Zhai H.Y., and Christen D.K., J. Mater. Res. **18** [4] 872-877 (2003).

[8] Paranthaman M., Goyal A., List F.A., Specht E.D., Lee D.F., Martin P.M., He Q., Christen D.K., Norton D.P., Budai J.D., Kroeger D.M., Physica C **275** 266-272 (1997).

[9] Rupich M., American Superconductor Corp, private communication.

[10] Wu L., Zhu Y., Solovyov V.F., Wiesmann H.J., Moodenbaugh A.R., Sabatini R.L., Suenaga M., J. Mater. Res. **16** [10] 2869 – 2884 (2001).

[11] Holesinger T.G., Gibbons B.J., Coulter J.Y., Foltyn S.R., Groves J.R., and Arendt P.N., Materials Research Society Symposium Proceedings Volume 689, *Materials for High-Temperature Superconductor Technologies*, Ed. M.P. Paranthaman, M.W. Rupich, K. Salama, J. Mannhart, and T. Hasegawa, Symposium held November 26-29, 2001, Boston, MA, 2002, pp. 329-336.

[12] Wong-Ng W., Cook L.P., Ceramic Transaction, 18, Superconductivity in Ceramic Superconductors 2, Nair K.M., Balachandran U., Chiang Y-M., Bhalla A., eds., Am. Ceram. Soc., Westerville, OH, 1991, pp. 73.

[13] Ritter J. J., Powd. Diffr. **3** 30-31 (1988).

[14] PDF, Powder Diffraction File, produced by International Centre of Diffraction Data (ICDD), 12 Campus Blvd., Newtown Squares, PA. 19073-3273.

[15] Larson A.C., von Dreele R.B. (1992). *GSAS-General Structure Analysis System*, US Government contract (W-7405-ENG-36) by the Los Alamos National Laboratory, which is operated by the University of California for the U.S. Department of Energy.

[16] Guha J.P., Kolar D., J. Mater. Sci. **6** (9) 1174-1177 (1971).

[17] Chase, Jr. M.W., NIST-JANAF Thermochemical Tables, 4th Edition, J. Phys. Chem. Ref. Data, Monograph No 9, 1998, pp.1952.

[18] Wang D.Y., Park D.S., Griffith J., Nowick A.S., Solid State Ionics **2** 95-105 (1981).

[19]Balazs G.B., Glass R.S., Solid State Ionics **76** 155-162 (1995).

[20]Longo V., Podda L., J. Mater. Sci. **16**(3) 839-841 (1981).

[21]Wong-Ng W., Yang Z., Cook L.P., Huang Q., Kaduk J.A.[1], and Frank J., Solid State Sciences, in print.

[22] Kingery W.D., Bower H.K., and Uhlmann D.R., *Introduction to Ceramics*, 2nd Ed., pp. 381-447, John Wiley & Sons, New York, USA, 1976.